Analysis of Ignition Mechanism of Combustible Mixtures by Short Duration Sparks

K.Ishii, M.Kono, K.Niu, T.Tsukamoto and Y.Ujiie

Department of Aeronautics
The University of Tokyo
3-1, Hongo 7-chome
Bunkyo-ku, Tokyo 113
Japan

ABSTRACT

Formation process of flame kernels produced by short duration sparks (less than 40 μs) in combustible mixtures is numerically simulated by using a model which considers heat release by chemical reaction. Simulation is done with emphasis on physical effects such as gas movement near spark gaps and heat transfer from the flame kernel to spark electrode surfaces. To estimate the effect of heat release, formation process of hot gas kernels in air is also simulated. The correctness of the present simulation is verified by experimental results. The calculated minimum ignition energy agrees qualitatively with the experimental one for various spark gap width, spark electrode diameter and spark duration. The calculated results show that the flame kernel configuration is governed by the gas flow pattern near the spark gap and that the flow pattern is affected by the spark electrode diameter, spark gap width and spark duration.

INTRODUCTION

Two important contributions have been given in recent fundamental studies of ignition of combustible mixtures by short duration sparks; one is related with capacitance sparks (1, 2) and the other breakdown sparks (3). The ignition mechanism by the former has been investigated because such sparks play an important role as a trigger of the following component of composite sparks (4, 5), which are conventional as ignition sparks for automobile engines. The latter is recommended as an ignition spark with good ability for automobile engines (6). It is reported in these works that the flame kernel produced by such short duration sparks has a toroidal shape (1-3, 7) in its incipient stage, namely in the ignition process which is estimated to be less than 200 μs after the spark discharge (2). Therefore, the toroidal development of flame kernels has close relations with ignition process, but the mechanism of formation of such toroidal kernel is unknown except for some estimation based on gas movement (2, 3) and ionic wind effect (7).

Present affiliation
* Mitsubishi Heavy Industry Co., Ltd.
** Institute of Fluid Science, Tohoku Univ.
*** College of Industrial Technology, Nihon Univ.

The authors have analyzed numerically the mechanism of flame kernel formation by short duration sparks (8). In Ref. (8) the toroidal flame kernel is well simulated by using the no heat release model. However, to calculate the value of the minimum ignition energy, it is necessary to consider heat release by chemical reaction.

In the present work, formation process of the flame kernels is numerically simulated by using a heat release model which considers the overall reaction. Simulation is done with emphasis on physical effects such as gas movement near spark gaps and heat transfer from the flame kernel to spark electrode surfaces. To estimate the effect of heat release, formation process of hot gas kernels in air is also simulated by using a no heat release model. Although the value of the calculated minimum ignition energy is different from that of the experimental, the effect of spark electrodes and spark duration is explained successfully.

MODEL DESCRIPTION

Formation process of flame kernels produced by short duration sparks in a stoichiometric propane-air mixture is numerically simulated by using the model which considers heat release by chemical reaction. Simulation is made with the partial differential equations for two dimensional cylindrical coordinates as shown in Appendix A. Figure 1 shows the coordinate system, the computing region and the location of the spark electrode. The flame kernel is assumed to be symmetric with respect to the z and r axes. The size of the region is 2 mm for both directions. To simplify the model, several assumptions are made: (1) Natural convection and heat transfer by radiation are neglected. (2) Chemical species are assumed to be propane, oxygen, nitrogen and combustion product, and an irreversible overall reaction is assumed. (3) Heat transfer from the flame kernel to the spark electrode surface, whose temperature is 300 K, is considered. (4) Prandtl number and Lewis number are unity.

The temperature dependency of Cp and ν is considered as

$$Cp/R = 3.33 - 3.61\times10^{-4}T + 5.06\times10^{-7}T^2 - 1.04\times10^{-11}T^3, \quad (1)$$

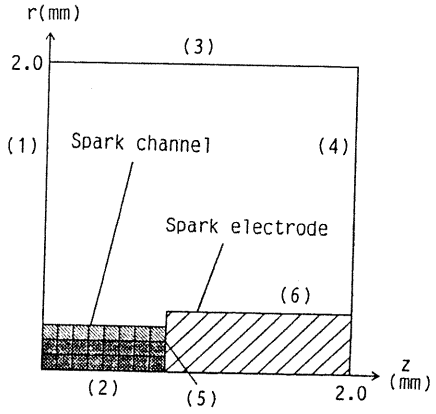

	E(J/cm^3)	ρ(kg/m^3)
▨	2.833 x $\frac{\text{time step}}{\text{spark duration}}$	1.199
▧	1.770 x $\frac{\text{time step}}{\text{spark duration}}$	1.199

Fig. 1. Region of simulation, notation of initial and boundary conditions.

$$\nu = -9.69\times10^{-6} + 6.32\times10^{-8}T + 6.99\times10^{-11}T^2. \quad (2)$$

The irreversible overall reaction is given by

$$C_3H_8 + 5O_2 + 18.8N_2 \rightarrow 7\text{Product} + 18.8N_2, \quad (3)$$

where the product is $3CO_2 + 4H_2O$. The reaction rate for the stoichiometric propane-air mixture is defined as

$$k = 0.4\times10^{8}\exp(-E/\bar{R}T)[C_3H_8]^{0.5}[O_2]^{0.5}. \quad (4)$$

For the determination of temperature, the following function, which has been obtained based on the assumption of chemical equilibrium of the combustion product, is used.

$$T = 64.8 + 1.28\times10^{-7}e - 1.83\times10^{-18}e^2 + 9.71\times10^{-30}e^3. \quad (5)$$

For the no heat release model, the equation like Eq. (5) is deduced from the assumption that air consists of nitrogen only.

The boundary conditions are as follows: In Fig. 2, for (1) and (2), the gradients of all variables are zero except that $v_z=0$ and $v_r=0$, respectively. For (3) and (4), the gradients of all variables are zero. For (5) and (6), no slip condition and heat transfer from the flame kernel to the spark electrode surface are assumed.

As for the initial condition, the temperature and pressure of the quiescent gas are respectively 300 K and 0.1 MPa except for within the spark channel which exists between the spark electrodes as shown in Fig. 1. A certain amount of energy is given in the spark channel for each time step. The initial value of pressure within the flame kernel is obtained from the velocity of the shock wave, which was measured beforehand, based on the simple shock wave theory (7). Then, the value of the temperature in the spark channel cell is calculated from the following equation of state,

$$p = \rho RT. \quad (6)$$

To deduce the minimum ignition energy in the simulation, there is need of change in the spark energy. In the experiment, it is observed that the luminous part of the spark channel becomes thick with increase in the spark energy. In calculation, thus, the radius of spark channel is changed according to the spark energy. Furthermore, the energy level of outer cells of the spark channel is changed in 4 staged value.

FLAME KERNEL STRUCTURE

Figure 2 shows calculated results of temperature distribution in a propane-air mixture. Immediately after spark discharge, the flame kernel is an ellipsoid and the high temperature region is located in the center of the spark gap. At 20 μs, the flame kernel is constricted near the tip ends of the spark electrodes. Afterwards, at 60 μs, the flame kernel is transformed into a torus and there is a groove inside the ring of the torus. At 100 μs, the ring grows and its center extends outward. These calculated results agrees well with schlieren photographs in Fig. 3.

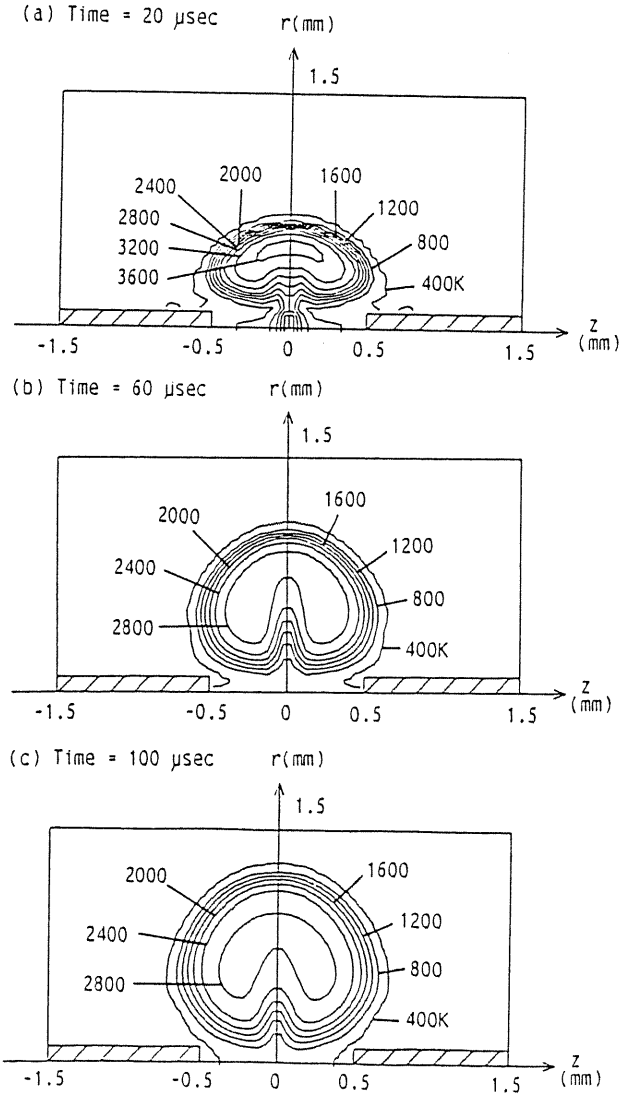

Fig. 2. Temperature distribution. Spark gap width: 1.0 mm; spark electrode: 0.2 mm in diam.

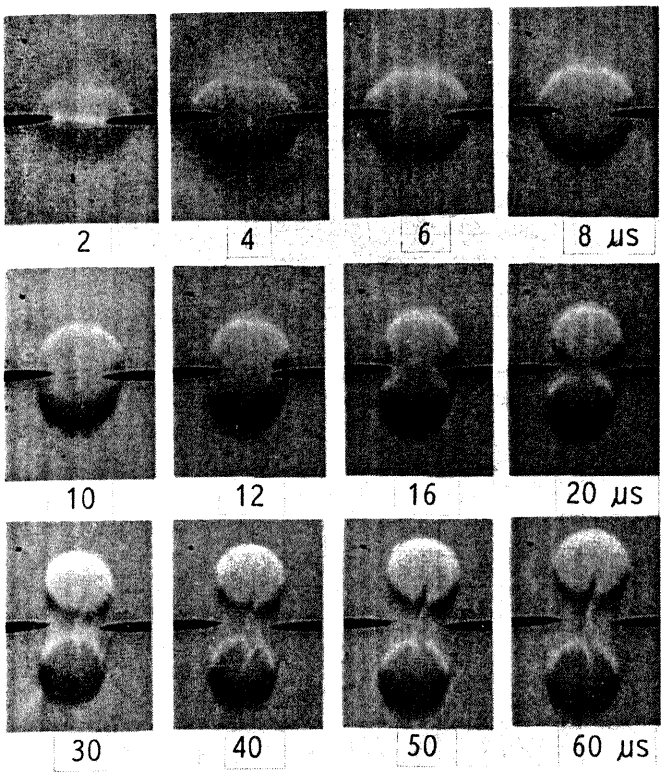

Fig. 3. Schlieren photographs of flame kernels. Spark gap width: 1.0 mm; spark electrode: 0.2 mm in diam.

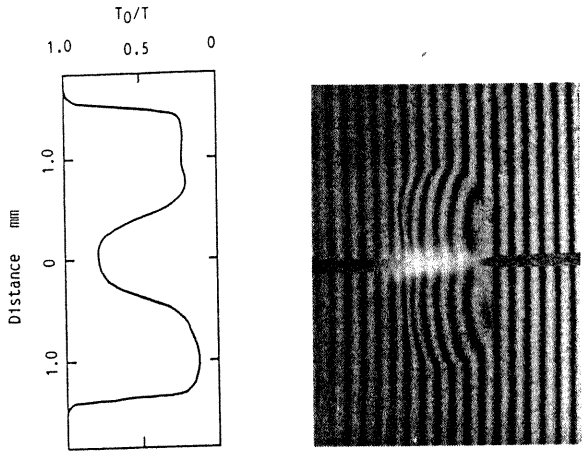

Fig. 4. Radial temperature distribution and corresponding interferogram of the flame kernel in a propane 4% (vol.)-air mixture at 42 μs after spark discharge. Spark gap width: 1.0 mm; spark electrode: 0.2 mm in diam.

To estimate the temperature distribution, interferometric measurement was carried out using a conventional Mach-Zender optical system. Figure 4 shows an example of the typical radial temperature distribution, which is obtained from the observed fringe shift in the interferogram of the flame kernel by using Abel inversion. The temperature has been normalized by the surrounding gas temperature (292 K). As can been seen, there is a low temperature region in the center of the spark gap. This confirms a toroidal shape of the flame kernel and verifies the calculated

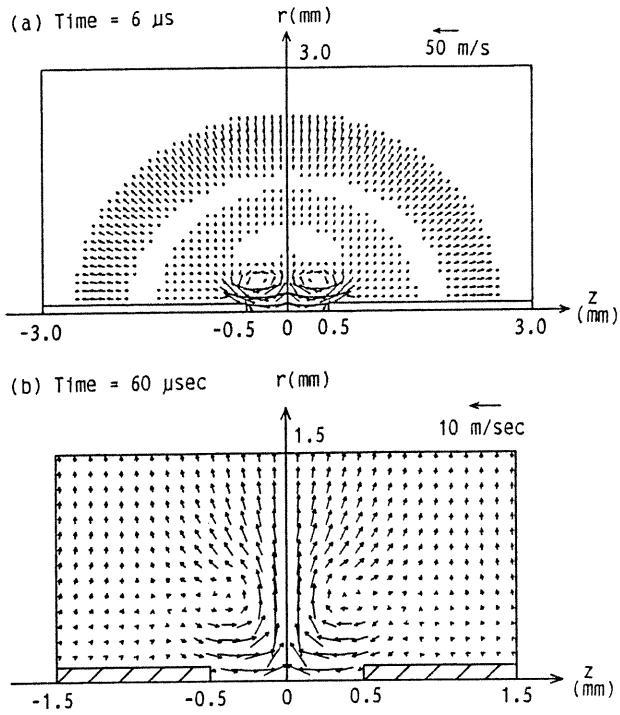

Fig. 5. Velocity distribution. Spark gap width: 1.0 mm; spark electrode: 0.2 mm in diam.

temperature distribution as shown in Fig. 2.

This formation process of the flame kernel can be explained by gas movement near the spark gap. Figure 5 shows calculated velocity distribution under the same condition as Fig. 2. In Fig. 5 (a), there can be seen a spherical shock wave produced by a sudden pressure rise in the spark gap. Inside the shock wave, a slight overexpansion raises an inward flow to the center of the spark gap. This flow carries the cold surrounding gas into the flame kernel and causes the constriction near the spark gap. In Fig. 5 (b), the inward flow along the spark electrode surfaces collides with each other and turns outwards. This gas motion moves the ring of the torus outward and also causes the groove inside the ring.

Figure 6 shows temperature distribution under no heat release condition and this corresponds to formation process of hot gas kernels in air. This formation process of the hot gas kernel is quite similar to that of the flame kernel in Fig. 2, though there is some differences in the absolute size of both kernels. The flame kernel is larger than the hot gas kernel because of heat release by chemical reaction and the toroidal ring of the flame kernel remains near the spark gap at 100 μs.

EFFECT OF SPARK ELECTRODE

As well known, the spark electrode affects the minimum ignition energy. Figure 7 shows the calculated and experimental minimum ignition energies. In calculation, the success in ignition is decided only if a flame kernel grows and reaches the boundary (1) or (2) in Fig. 1. The calculated minimum ignition energy is defined by the minimum value of the spark energy which causes successful ignition. Although there is a difference in the absolute value of the minimum ignition energy between the calculated and the

experimental results, the dependency on spark electrode diameter agrees well with each other. This dependency can be well explained by the present simulation. In the case of 1.0 mm gap width, for smaller electrode diameters less than 0.3 mm, the flame kernel remains near the spark gap as shown in Fig. 2. Thus, the flame kernel is strongly quenched by the spark electrode, so that the minimum ignition energy increases rapidly with increasing electrode diameter. For electrodes thicker than 0.3 mm, the flame kernel is divided into two parts as shown in Fig 8. As time elapses, the high temperature region in the spark gap is extinguished because of the heat loss to the spark electrode. Then, the spark energy in the torus may not change, and thus the minimum ignition energy depends slightly on the spark electrode diameter. In the case of 3.0 mm gap

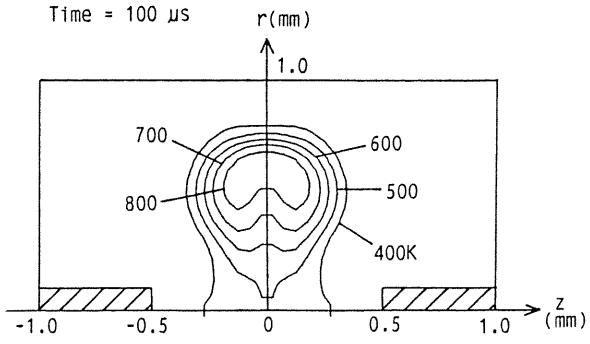

Fig. 6. Temperature distribution. Spark gap width: 1.0 mm; spark electrode: 0.2 mm in diam.

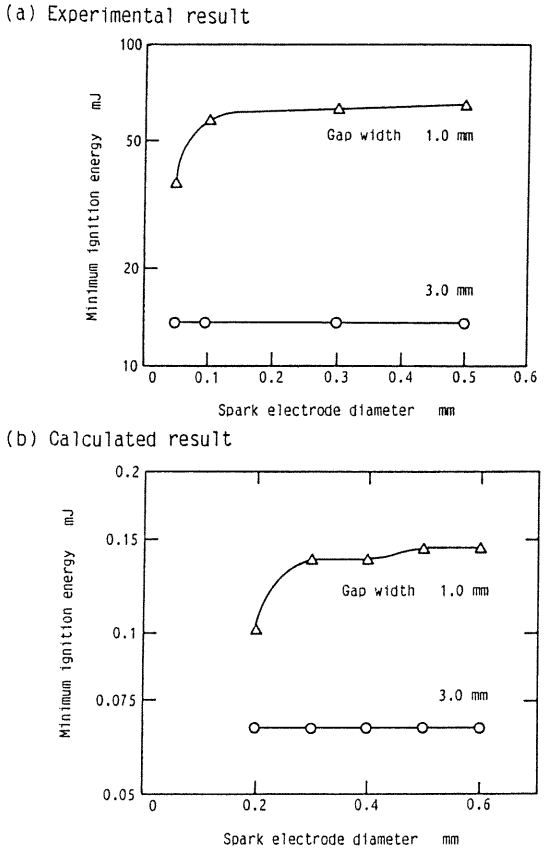

Fig. 7. Effect of spark electrode diameter and gap width on minimum ignition energy.

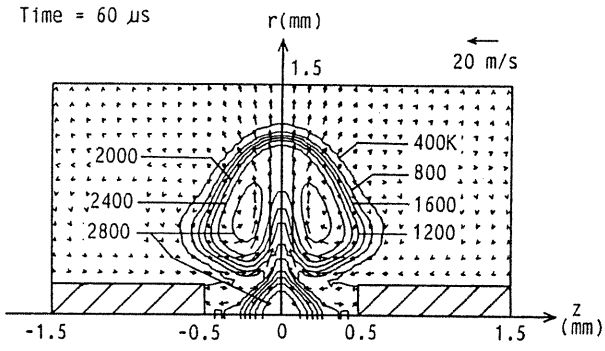

Fig. 8. Temperature and velocity distributions. Spark gap width: 1.0 mm; spark electrode: 0.4 mm in diam.

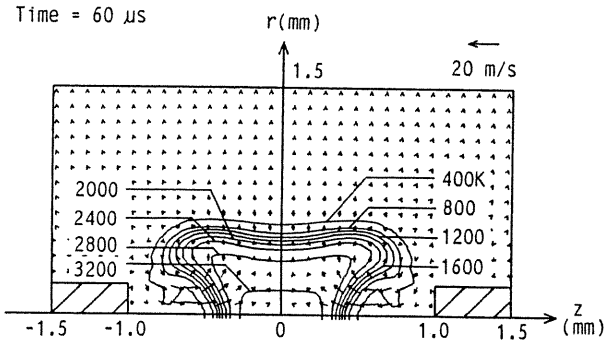

Fig. 9. Temperature and velocity distributions. Spark gap width: 2.0 mm; spark electrode: 0.4 mm in diam.

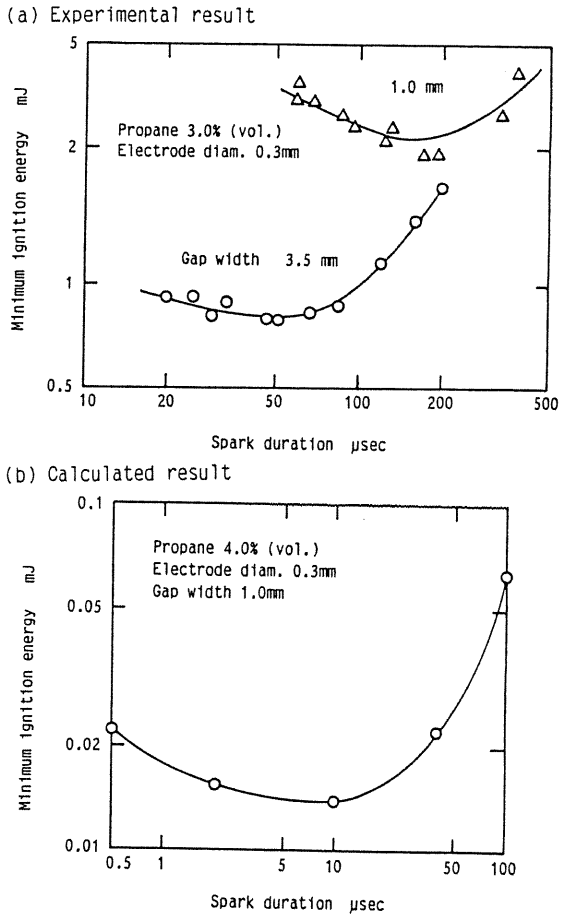

Fig. 10. Effect of spark duration on minimum ignition energy.

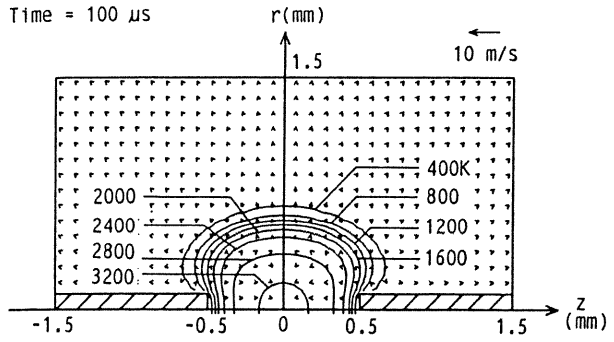

Fig. 11. Temperature and velocity distributions. Spark gap width: 1.0 mm; spark electrode: 0.2 mm in diam.; spark duration: 10 μs.

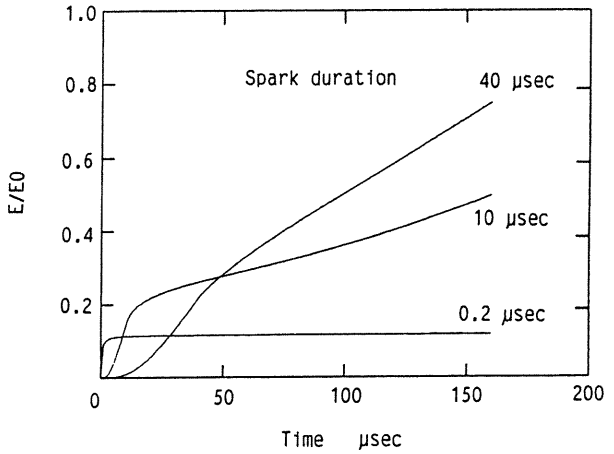

Fig. 12. Ratio of heat loss (E) to spark electrode to spark energy (E0). Spark gap width: 1.0 mm; spark electrode: 0.2 mm in diam.

width, the high temperature region is formed away from the spark electrode as shown in Fig. 9. Therefore, the spark electrode has little effect on quenching of the flame kernel, and then, the minimum ignition energy remains constant for various electrode diameters.

EFFECT OF SPARK DURATION

Figure 10 shows the calculated and experimental minimum ignition energies for different spark durations. For both results, the existence of optimum spark duration, for which the minimum ignition energy is the lowest, can be seen. The reason why the optimum spark duration appears is successfully given by using the present simulation as follows: Figure 11 shows temperature and velocity distributions for 10 μs spark duration. The flame kernel is still ellipsoid at 100 μs compared with the toroidal flame kernel as shown in Fig 2 (c). The high temperature region is located in the center of the spark gap, and thus, it is estimated that the heat loss to the spark electrode is more than that for shorter spark duration. Figure 12 shows the calculated heat loss to the spark electrode for various spark duration, where E and E0 are the heat loss and the spark energy, respectively. The increment of the heat loss causes the minimum ignition energy to increase for spark duration longer than 10 μs. For spark duration shorter than 10 μs, a part of the spark energy is removed by the shock wave which occurs right after the spark discharge. Additionally, the flame kernel is cooled by the cold surrounding gas which flows into the flame kernel. Therefore, minimum ignition energy increases with decreasing spark duration.

CONCLUSION

Formation process of flame kernels produced by short duration sparks is numerically simulated by using the heat release model. The conclusions we find are as follows:
(1) The minimum ignition energy can be successfully calculated for various spark gap width, spark electrode diameter and spark duration.
(2) The flame kernel configuration is governed by the flow pattern near the spark gap. The flow pattern is affected by the spark electrode diameter, gap width and spark duration.
(3) For the flame kernel structure, the calculated results agree well with the experimental one on the basis of schlieren photographs and interferometry.
(4) The calculated minimum ignition energy agrees qualitatively with the experimental one.

NOMENCLATURE

Cp: specific heat at constant pressure, J/(kgK)
E: activation energy, J/mol
e: specific internal energy, J/kg
h: specific enthalpy, J/kg
k: reaction rate, mol/(m^3s)
q: energy flux, J/(m^2s)
$\dot{q}$: heat release rate, J/(m^3s)
R: gas constant, J/(kgK)
$\bar{R}$: universal gas constant, J/(molK)
r: radial coordinate, m
T: temperature, K
t: time, s; v: velocity, m/s
Y: mass fraction
z: axial coordinate, m
κ: thermal conductivity, J/(m^2s K)
μ: viscosity, kg/(m s)
ν: kinematic viscosity, kg/(ms)
ρ: density, kg/m^3
$\dot{\rho}$: production rate, kg/(m^3s)
τ: stress tensor, Pa

Subscripts
c: chemical
i: species
r: radial component
z: axial component
θ: angle in spherical coordinates

REFERENCES

1. Kono, M. and Hatori, K., "IGNITION OF LOW FLOW VELOCITY MIXTURES BY SHORT DURATION SPARKS," Eighth International Conference of Gas Discharges and their Applications, pp. 500-503, 1985.
2. Kono, M., Kumagai, S. and Sakai, T., "Ignition of Gases by Two Successive Sparks with Reference to Frequency Effect of Capacitance Sparks," Combustion and Flame, Vol. 27, pp. 85-98, 1976.
3. Maly, R. and Vogel, M., "INITIATION AND PROPAGATION OF FLAME FRONTS IN LEAN CH_4-AIR MIXTURES BY THE THREE MODES OF THE IGNITION SPARK," Seventeenth Symposium (International)

on Combustion, The Combustion Institute, pp. 821-831, 1979.
4. Kono, M., Kumagai, S. and Sakai, T., "THE OPTIMUM CONDITION FOR IGNITION OF GASES BY COMPOSITE SPARKS," Sixteenth Symposium (International) on Combustion, The Combustion Institute, pp. 757-766, 1977.
5. Kono, M., Hatori, K. and Iinuma, K., "INVESTIGATION ON IGNITION ABILITY OF COMPOSITE SPARKS IN FLOWING MIXTURES," Twentieth Symposium (International) on Combustion, The Combustion Institute, pp. 133-140, 1985.
6. Ziegler, G. F. W., Wagner, E. P., Saggau, B., Maly, R. and Herden, W., "Influence of a Breakdown Ignition System on Performance and Emission Characteristics," SAE Transactions, Vol. 93, Paper No. 840992, pp. 643-655, 1984.
7. Olsen, H. L., Edmonson, R. B. and Gayhart, E. L., "Microchronometrtic Schlieren Study of Gaseous Expansion from an Electric Spark," Journal of Applied Physics, Vol. 23, pp 1157-1162, 1952.
8. Kono, M., Niu, K., Tsukamoto, T and Ujiie, Y., "MECHANISM OF FLAME KERNEL FORMATION PRODUCED BY SHORT DURATION SPARKS," Twenty-Second Symposium (International) on Combustion, The Combustion Institute, pp. 1643-1649, 1989.
9. Rivard, W. C., Farmer, O. A., and Butler, T. D., "RICE: A Computer Program for Multicomponent Chemically Reactive Flows at All Speeds," Los Alamos Scientific Laboratory Report, LA-5812, 1975.

APPENDIX A

The partial differential equations for two dimensional cylindrical coordinates are as follows:

Mass conservation:

$$\frac{\partial \rho}{\partial t} + \frac{1}{r}\frac{\partial \rho v_r r}{\partial r} + \frac{\partial \rho v_z}{\partial z} = 0. \tag{A1}$$

Momentum conservation:

$$\frac{\partial \rho v_r}{\partial t} + \frac{1}{r}\frac{\partial \rho v_r^2 r}{\partial r} + \frac{\partial \rho v_z v_r}{\partial z} = -\frac{\partial p}{\partial r} - \frac{1}{r}\frac{\partial \rho v_r v_z r}{\partial r} + \frac{\tau_{\theta\theta}}{r} - \frac{\partial \tau_{rz}}{\partial z}, \tag{A2}$$

$$\frac{\partial \rho v_z}{\partial t} + \frac{1}{r}\frac{\partial \rho v_r v_z}{\partial r} + \frac{\partial \rho v_z^2}{\partial z} = -\frac{\partial p}{\partial z} - \frac{1}{r}\frac{\partial \tau_{rz} r}{\partial r} - \frac{\partial \tau_{zz}}{\partial z}. \tag{A3}$$

Energy conservation:

$$\frac{\partial \rho e_t}{\partial t} + \frac{1}{r}\frac{\partial \rho v_r e_t r}{\partial r} + \frac{\partial \rho v_z e_t}{\partial z} = -\frac{1}{r}\frac{\partial q_r r}{\partial r} - \frac{\partial q_z}{\partial z} - \frac{1}{r}\frac{\partial p v_r r}{\partial r} - \frac{\partial p v_z}{\partial z} - \frac{1}{r}\frac{\partial}{\partial r}(\tau_{rr} v_r r + \tau_{rz} v_z r) - \frac{\partial}{\partial z}(\tau_{rz} v_r + \tau_{zz} v_z) + \dot{q}_c. \tag{A4}$$

Species conservation:

$$\frac{\partial \rho_i}{\partial t} + \frac{1}{r}\frac{\partial \rho_i v_r r}{\partial r} + \frac{\partial \rho_i v_z}{\partial z} = \frac{1}{r}\frac{\partial}{\partial r}(\rho D \frac{\partial Y_i}{\partial r} r) + \frac{\partial}{\partial z}(\rho D \frac{\partial Y_i}{\partial z}) + (\dot{\rho}_i)_c, \tag{A5}$$

where,

$$\tau_{rr} = -\mu(2\frac{\partial v_r}{\partial r} - \frac{2}{3}(\frac{1}{r}\frac{\partial v_r r}{\partial r} + \frac{\partial v_z}{\partial z})), \tag{A6}$$

$$\tau_{\theta\theta} = -\mu(2\frac{v_r}{r} - \frac{2}{3}(\frac{1}{r}\frac{\partial v_r r}{\partial r} + \frac{\partial v_z}{\partial z})), \tag{A7}$$

$$\tau_{zz} = -\mu(2\frac{\partial v_z}{\partial z} - \frac{2}{3}(\frac{1}{r}\frac{\partial v_r r}{\partial r} + \frac{\partial v_z}{\partial z})), \tag{A8}$$

$$\tau_{rz} = -\mu(\frac{\partial v_r}{\partial r} + \frac{\partial v_z}{\partial z}), \tag{A9}$$

$$q_r = -\kappa\frac{\partial T}{\partial r} - \sum_{i=1}^{n} \rho_i h D \frac{\partial Y_i}{\partial r}, \tag{A10}$$

$$q_z = -\kappa\frac{\partial T}{\partial z} - \sum_{i=1}^{n} \rho_i h D \frac{\partial Y_i}{\partial z}, \tag{A11}$$

$$e_t = e + \frac{1}{2}(v_r^2 + v_z^2), \tag{A12}$$

$$h = e + \frac{p}{\rho}. \tag{A13}$$

The partial differential equations, Eqs. (A1)-(A5), are solved by a part of RICE code (9). Briefly, Eqs. (A1)- (A3) are solved in an iterative manner by a first order implicit scheme. Then Eqs. (A4) and (A5) are solved by an explicit scheme and afterward the values of internal energy and density are updated. The final pressure is determined from Eq. (6). The numerical stability is satisfied by considering the discussion in Ref. (9). Based on this, the cell size and the time step are decided as 0.05 mm and 0.02 μs, respectively.